RSC Advances

PAPER

View Article Online
View Journal | View Issue

Cite this: *RSC Adv.*, 2024, **14**, 24175

Fabrication of magnetic carbohydrate-modified iron oxide nanoparticles (Fe_3O_4/pectin) decorated with bimetallic Co/Cu-MOF as an effective and recoverable catalyst for the Biginelli reaction

Majid Grami and Zahra Rafiee *

Due to their biocompatibility, facile recoverability, mechanical and thermal stability, high surface area, and active catalytic sites, magnetic nanocomposites, containing natural polymers and magnetic nanoparticles, have been used to produce supports for catalysts or biocatalysts. Pectin, an important polycarbohydrate, has abundant functional groups with excellent ability to coat the surface of the nanoparticles to fabricate composite and hybrid materials. A novel bimetallic cobalt(II) and copper(II)-based metal–organic framework (Co/Cu-MOF) immobilized pectin-modified Fe_3O_4 magnetic nanocomposite was designed and fabricated. Fe_3O_4 nanoparticles were modified *in situ* by pectin and, subsequently, used as a support for growing Co/Cu-MOF [Fe_3O_4/pectin/(Co/Cu)MOF]. The properties of the nanocomposite were investigated by FT-IR, XRD, SEM, EDS, VSM, STA, and BET. The nanocomposite exhibited both magnetic characteristics and a high surface area, making it a suitable candidate for catalytic applications. Then, the Fe_3O_4/pectin/(Co/Cu)MOF nanocomposite was utilized in the Biginelli reaction for the production of biologically active dihydropyrimidinones. Due to paramagnetism, Fe_3O_4/pectin/(Co/Cu)MOF was easily recovered and reused in six cycles without significant loss in reactivity. This green method comprises several benefits, such as mild reaction conditions, free-solvent media, high yields, easy workup, short reaction times and reusability of the prepared catalyst.

Received 29th April 2024
Accepted 18th July 2024

DOI: 10.1039/d4ra03182b

rsc.li/rsc-advances

1. Introduction

The Biginelli reaction represents incredibly significant multi-component reactions that generate bioactive compounds with various therapeutic and pharmacological traits, such as anti-tumor, antibacterial, and antioxidant.[1–3] The Biginelli reaction includes the three-component, acid-catalyzed condensation of aldehydes, β-ketoester, and urea to yield dihydropyrimidones.[4–10] So far, various compounds, including Brønsted or Lewis acids and ionic liquids, have been utilized to catalyze the Biginelli reaction.[4–11]

Magnetic nanoparticles (MNPs) have attracted considerable interest as exceptional supports for immobilization, owing to the presence of abundant surface hydroxyl groups, highly stable, straightforward accessibility, great permeability, inexpensiveness, and easy separation using an external magnet.[12–14] The surface of MNPs can be functionalized by a variety of polymers.[15,16] Among them, biopolymers receive special attention because of their biocompatibility and biodegradability.[17,18] Pectin, as a natural biopolymer, is a water-soluble gelatin-like material and is known as one of the structurally complicated members of polycarbohydrates abundant in the cell walls of plants with key roles in primary/secondary structure of the wall and its function.[19] Carbohydrate-based coatings, especially coating by pectin, on the surface of various nanoparticles, liposomes, foods and materials have recently attracted the attentions of scientists due to the ability of carbohydrates to enhance the physicochemical and/or storage stability of the materials, or adding specific functions for different purposes such as drug delivery. Pectin possesses valuable properties, such as the availability of plenteous carboxyl and hydroxyl functional groups, non-toxicity, low-cost, high flexibility, and biodegradability that has made it an outstanding biomolecule for use in surface engineering nanotechnology.[20]

Metal–organic frameworks (MOFs) represent a class of porous crystalline materials, constructed from metal ions or metal oxide clusters bridged by organic linkers that exhibit substantial porosity, high surface area, and diverse functionalities.[21,22] MOFs are of special interest owing to their extensive range of potential applications, such as catalysis, medicinal, gas storage, separation, and chemical sensors.[23–31] However, the actual application of MOFs has been hampered by their poor stability, chemical instability, and difficult recovery. Recently, composites based on MOFs have been constructed by the

Department of Chemistry, Yasouj University, Yasouj, 75918-74831, Iran. E-mail: z.rafiee@yu.ac.ir; zahrarafiee2004@yahoo.com; Fax: +98-741-222-3048; Tel: +98-741-222-3048

combination of MOFs with materials including metal nanoparticles, quantum dots, natural enzymes, and polymers, which represent physical and chemical properties that are superior to those of the individual components, due to the combination of features from the two ingredients.[32,33] The combination of functionalized magnetic nanoparticles and MOFs creates magnetic porous composites, which have attracted considerable attention due to a large number of advanced applications in diverse fields.[34] These magnetic porous composites possess a core–shell architecture containing a porous shell on the magnetic core. The resulting nanostructures presented magnetic properties and high surface area without aggregation of magnetite cores, enabling them to become desired candidates for the catalysts of organic reactions.[35] Bimetallic MOFs are MOFs comprising two various metal ions in their frameworks. These MOFs can be easily fabricated using the mixture of different metals *via* two synthetic methods: the one-pot synthesis method or the post-synthetic ion exchange method.[36–38] These mixed-metal MOFs represent a superior catalytic activity compared to the corresponding single-metal MOFs, owing to the existence of two different metal active sites, which are suitable for orthogonal and multicomponent reactions as well as other synthetic routes requiring advanced multisite catalysts.[39,40]

In the present work, Fe_3O_4/pectin/(Co/Cu)MOF nanocomposite was hydrothermally prepared and utilized as an effective and cost-effective heterogeneous catalyst for the Biginelli reaction under solvent-free conditions. The synergistic effects of Fe_3O_4, Co-MOF, and Cu-MOF are expected to enhance catalytic performance.

2. Experimental

2.1. Materials

The reagents and chemicals including iron(II) chloride tetrahydrate ($FeCl_2 \cdot 4H_2O$), iron(III) chloride hexahydrate ($FeCl_3 \cdot 6H_2O$), sodium hydroxide (NaOH), urea ($CO(NH_2)_2$), ethyl acetoacetate, cobalt(II) nitrate hexahydrate ($Co(NO_3)_2 \cdot 6H_2O$), copper(II) nitrate trihydrate ($Cu(NO_3)_2 \cdot 3H_2O$), 1,4-benzenedicarboxylic acid (1,4-BDC, terephthalic acid), *N*,*N*-dimethylformamide (DMF), ethanol, benzaldehyde, 4-nitrobenzaldehyde, 4-chlorobenzaldehyde, 2-chlorobenzaldehyde, 4-methoxybenzaldehyde, 4-methylbenzaldehyde, and 2-hydroxybenzaldehyde were purchased from Merck Company (Darmstadt, Germany) and used without further purification. Pectin was supplied by Lidoma Golden Day Ltd company (Tehran, Iran).

2.2. Apparatus

FT-IR spectra were recorded with a Jasco-680 spectrometer (Japan) in the range of 4000–400 cm^{-1}. FT-IR spectra of the compounds were collected by making their pellets in KBr, as a medium. The X-ray diffraction pattern of the prepared materials was recorded in the reflection mode using a Bruker, D8 Advance diffractometer. The ultrasonic bath (Tecno-GAZ SPA Ultrasonic system, Italy) was used at a frequency of 60 Hz and power of 130 W. The surface morphology of the nanocomposite was examined by scanning electron microscopy (SEM; EM10C-ZEISS, 80 kV, Zeiss Co., Germany). Nitrogen adsorption/desorption isotherm was measured by Brunauer–Emmett–Teller analysis (Belsorp Mini II, Japan). The thermal stability of the nanocomposite was determined by Simultaneous Thermal Analyzer (STA, PerkinElmer STA6000, USA).

2.3. Preparation of Fe_3O_4/pectin

1.00 g of pectin was dissolved in 100 mL of distilled water under continuous stirring at room temperature. In another vessel, 5.00 g of $FeCl_3 \cdot 6H_2O$ and 2.00 g of $FeCl_2 \cdot 4H_2O$ were dissolved in 10 mL of distilled water. The solutions were mixed, and then the pH of the solution increased to 12 with NaOH. Finally, the mixture was stirred at 80 °C for 1 h and then cooled to room temperature. The resultant precipitate was collected through an external magnet, washed with deionized water and ethanol, and dried at 70 °C under vacuum.

2.4. Synthesis of Fe_3O_4/pectin/(Co–Cu)MOF

0.3 g of Fe_3O_4/pectin was dispersed in 30 mL of DMF under ultrasound irradiation for 20 min. Consequently, 0.1 g of $Co(NO_3)_2 \cdot 6H_2O$, 0.09 g of $Cu(NO_3)_2 \cdot 3H_2O$, and 0.13 g of 1,4-BDC were added to the above mixture and sonicated for 30 min. The mixture was placed in a 150 mL Teflon-lined autoclave and heated up to 140 °C for 48 h, then cooled back down to room temperature. The dark brown precipitate was collected using an external magnet, washed with ethanol, and dried at 70 °C under vacuum.

2.5. The Biginelli reaction using Fe_3O_4/pectin/(Co–Cu)MOF as a catalyst

General procedure: a mixture of aldehydes (1.0 mmol), ethyl acetoacetate (1.0 mmol), urea (1.5 mmol), and Fe_3O_4/pectin/(Co–Cu)MOF (25 mg) was stirred under solvent-free conditions at 85 °C. The progress of the reaction was monitored by thin-layer chromatography (TLC). After the reaction was completed, warm ethanol (10 mL) was added to the reaction mixture and Fe_3O_4/pectin/(Co–Cu)MOF was separated using a magnet and washed with ethanol. The solvent was evaporated and the solid was recrystallized from ethanol to produce the pure product. The products were identified by matching their melting points and FT-IR analysis. The recovered Fe_3O_4/pectin/(Co–Cu)MOF was reused in six runs under similar conditions as the first run to reveal the recyclability and stability of the catalyst.

5-(Ethoxycarbonyl)-6-methyl-4-phenyl-3,4-dihydropyrimidin-(1H)-one (4a): m.p.: 202–204 °C. ^{1}H NMR (400 MHz, DMSO-d_6) δ 9.27 (s, 1H), 7.89 (s, 1H), 7.47 (t, 2H), 7.58 (d, 3H), 5.32 (d, J = 3.4 Hz, 1H), 3.83 (q, J = 7.3 Hz, 2H), 2.21 (s, 3H), 1.12 (t, J = 7.3 Hz, 3H).

5-(Ethoxycarbonyl)-6-methyl-4-(4-nitrophenyl)-3,4-dihydropyrimidin-2(1H)-one (4b): m.p.: 202–203 °C. ^{1}H NMR (400 MHz, DMSO-d_6) δ 9.42 (s, 1H), 8.53 (d, J = 8.9 Hz, 2H), 7.86 (s, 1H), 7.63 (d, J = 8.9 Hz, 2H), 5.48 (d, J = 3.4 Hz, 1H), 3.76 (q, J = 7.4 Hz, 2H), 2.22 (s, 3H), 1.25 (t, J = 7.1 Hz, 3H).

5-(Ethoxycarbonyl)-6-methyl-4-(2-chlorophenyl)-3,4-dihydropyrimidin-2(1H)-one (4d): m.p.: 221–223 °C. ^{1}H NMR (400 MHz, DMSO-d_6) δ 9.47 (s, 1H), 7.68 (s, 1H), 7.13–7.38 (m, 4H), 5.71 (d, $J = 2.8$ Hz, 1H), 3.92 (q, $J = 7.4$ Hz, 2H), 2.41 (s, 3H), 0.89 (t, $J = 7.4$ Hz, 3H).

3. Results and discussion

3.1. Synthesis of Fe_3O_4/pectin/(Co–Cu)MOF

The synthesis of Fe_3O_4/pectin/(Co–Cu)MOF for the Biginelli reaction was reported using commercially available chemical materials. Pectin is a natural biopolymer that is obtained from many fruits. This biopolymer is a polysaccharide containing carboxylic acid groups in each monomer. The carboxylic acid groups on the surface of pectin are covalently chelated to Fe_3O_4 nanoparticles and direct the nanostructure. Moreover, pre-treating Fe_3O_4 nanoparticles with pectin improved their compatibility with MOFs and facilitated the growth of MOFs around Fe_3O_4 nanoparticles. Fe_3O_4/pectin was treated with $Co(NO_3)_2 \cdot 6H_2O$ and $Cu(NO_3)_2 \cdot 3H_2O$ (as inorganic constituents), 1,4-BDC, and DMF (as a solvent) *via* heating to 140 °C for 48 h to form Fe_3O_4/pectin/(Co–Cu)MOF nanocomposite. The synthesis route of Fe_3O_4/pectin/(Co–Cu)MOF nanocomposite is displayed in Fig. 1.

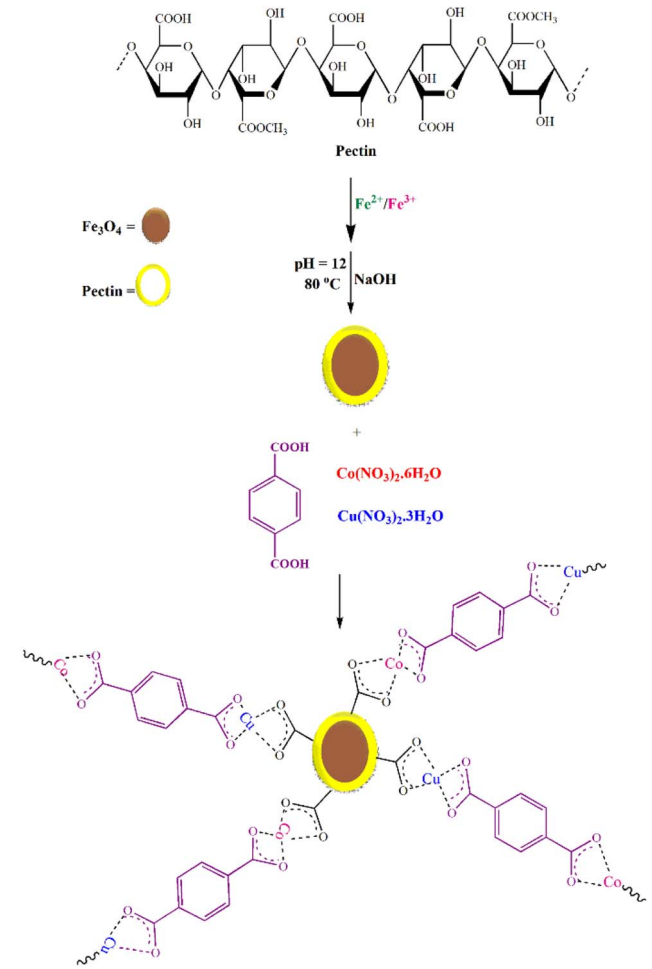

Fig. 1 Preparation of Fe_3O_4/pectin/(Co/Cu)MOF nanocomposite.

3.2. Characterization of the prepared compounds

Fig. 2 displays the FT-IR spectra of pectin (a), Fe_3O_4/pectin (b), (Co/Cu)MOF (c) and Fe_3O_4/pectin/(Co/Cu)MOF (d). In the FT-IR spectrum of pectin, the bands at 3389, and 2932 cm^{-1} are attributed to the stretching vibrations of O–H and C–H bonds, respectively. The peak which appeared around 1760 cm^{-1} corresponds to C=O stretching vibration. The peak at 1626 cm^{-1} is assigned to the bending vibration of O–H and the peak around 1120 cm^{-1} is related to the stretching vibration of

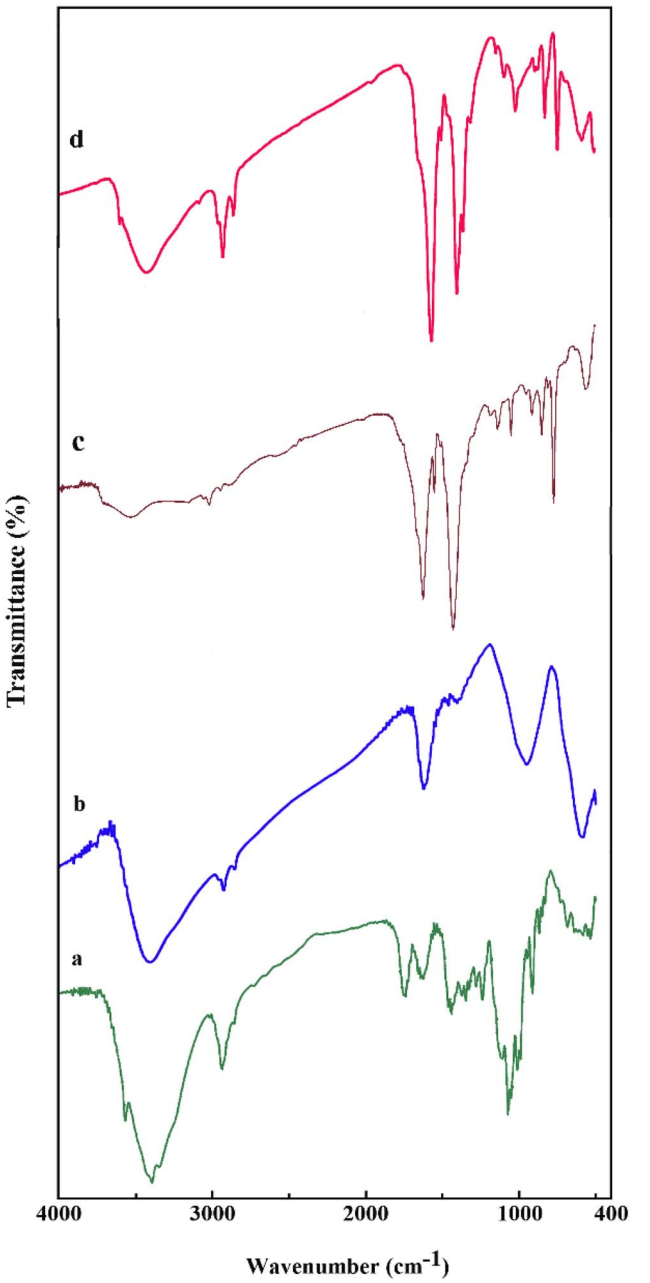

Fig. 2 FT-IR spectra of pectin (a), Fe_3O_4/pectin (b), (Co/Cu)MOF (c) and Fe_3O_4/pectin/(Co/Cu)MOF (d).

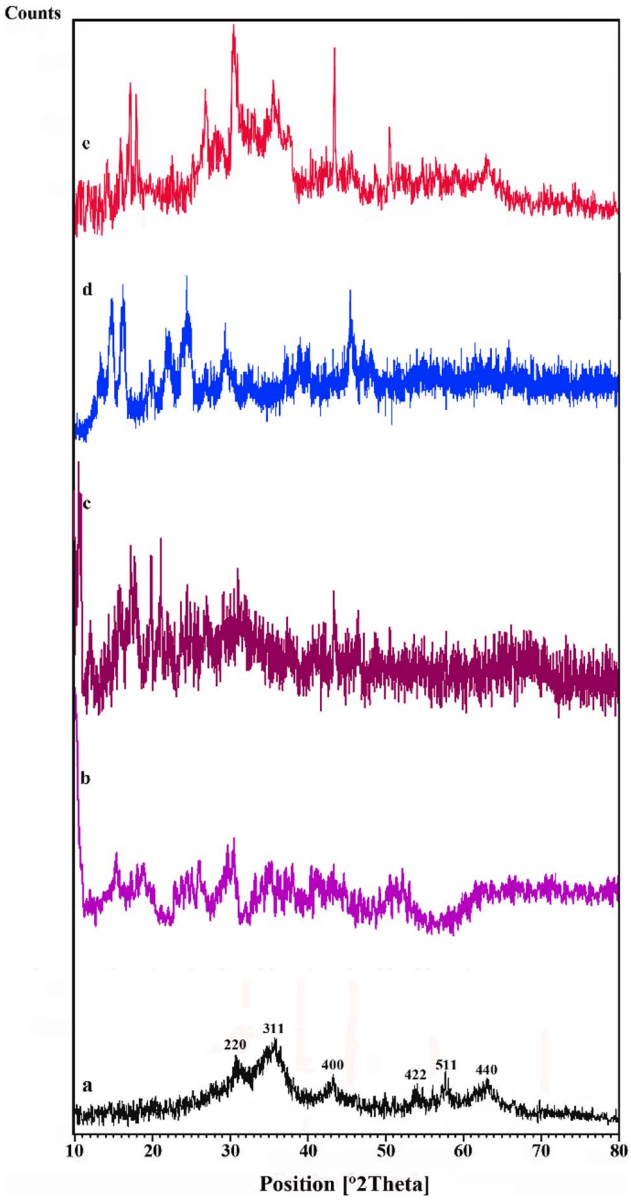

Fig. 3 XRD patterns of Fe_3O_4/pectin (a), Co-MOF (b), (Co/Cu)MOF (c), Cu-MOF (d), Fe_3O_4/pectin/(Co/Cu)MOF (e).

C–O. In the spectrum of Fe_3O_4/pectin, the absorption peaks at 3401, 2932, 1620, and 584 cm^{-1} are related to the stretching vibrations of O–H, C–H, C=O, and Fe–O bonds, respectively. In the spectrum of (Co–Cu)MOF, the two absorption peaks appeared at 1620 and 1434 cm^{-1} correspond to the asymmetric and symmetric stretching vibrations of the O=C–O bonded to Cu and Co. The peak appeared at 597 cm^{-1} in the spectrum of Fe_3O_4/pectin/(Co–Cu)MOF nanocomposite is attributed to Fe–O stretching vibration, and the absorption peaks observed at 1563 and 1400 cm^{-1} correspond to the asymmetric and symmetric stretching of the O=C–O bonded to Co and Cu metals.

Fig. 3 represents the XRD patterns of Fe_3O_4/pectin (a), Co-MOF (b), (Co/Cu)MOF (c), Cu-MOF (d), and Fe_3O_4/pectin/(Co/Cu)MOF (e). As can be seen, the XRD profile of Fe_3O_4/pectin/(Co/Cu)MOF reflects the characteristic peaks of standard cubic spinel Fe_3O_4 nanoparticles that appeared at $2\theta = 30.4°$, 35.9°, 43.2°, 54.1°, 57.2° and 63.1°. These correspond to the (220), (311), (400), (422), (511) and (440) diffraction planes (JCPDS No. 19–0629). However, the additional peaks observed at $2\theta = 14.3°$, 15.0°, 17.1°, 18.0°, 22.5°, 25.2°, 27.9°, 28.7°, 35.5°, 47.7°, 48.8° and 50.5° are assigned to Co-MOF and Cu-MOF crystalline phases.

The surface morphology of Fe_3O_4/pectin/(Co–Cu)MOF nanocomposite was investigated by scanning electron microscopy (SEM). The SEM images showed that the Fe_3O_4/pectin/(Co–Cu)MOF nanocomposite possesses nanoparticles with spherical morphology with uniform shapes and smooth surface (Fig. 4). In addition, the EDS analysis of the prepared catalyst confirms the existence of Co and Cu in the framework. It displays the presence of carbon, oxygen and iron atoms (Fig. 5).

The thermal stability of Fe_3O_4/pectin/(Co–Cu)MOF nanocomposite was examined by simultaneous thermal analysis (STA, Fig. 6). The first weight loss that appeared in a temperature range of 210–400 °C can be attributed to the removal of immobilized pectin groups onto the Fe_3O_4 surface. The second weight loss from 420 to 550 °C is related to the degradation of pectin and the decomposition of MOF shells on the material surface. These data successfully prove the good thermal stability of Fe_3O_4/pectin/(Co–Cu)MOF at 200 °C, demonstrating its sufficient stability for catalytic applications.

The magnetic property of Fe_3O_4/pectin/(Co–Cu)MOF was measured by a vibrating sample magnetometer (VSM). The saturation magnetization of Fe_3O_4/pectin/(Co–Cu)MOF nanocomposite is about 7 emu g^{-1} (Fig. 7), which is lower than that of Fe_3O_4 (about 65 emu g^{-1}). This decrease in saturation magnetization confirms the successful coating of (Co/Cu)MOF shell on the surface of the Fe_3O_4 nanoparticles. Also, the magnetic isolating of Fe_3O_4/pectin/(Co–Cu)MOF nanocomposite is tested by setting a magnet near the glass bottle of the nanocomposite.

The porosity of Fe_3O_4/pectin/(Co–Cu)MOF is examined by measuring N_2 adsorption–desorption isotherms at 77 K. According to this analysis, the surface area, the total pore volume, and the mean diameter of the cavities were 207 $m^2 g^{-1}$, 0.1756 $cm^3 g^{-1}$, and 6.591 nm, respectively (Fig. 8).

3.3. Catalytic activity test

The catalytic activity of Fe_3O_4/pectin/(Co–Cu)MOF was tested in the reaction of benzaldehyde, ethyl acetoacetate, and urea as a model reaction (Table 1). The effect of catalyst loading was investigated by carrying out the model reaction in the presence of different amounts of Fe_3O_4/pectin/(Co–Cu)MOF. Upon increasing the amount of catalyst from 10 to 25 mg, a noteworthy increase in the yield of the product was observed (Table 1, entries 2–5), which proves that the progress of the reaction is affected by the catalyst loading. By increasing the catalyst loading to 30 mg, no significant change in the yield of the product is observed (Table 1, entry 6). The best amount of Fe_3O_4/pectin/(Co–Cu)MOF is 25 mg which created the desired product with 96% yield (Table 1). The reaction was also affected

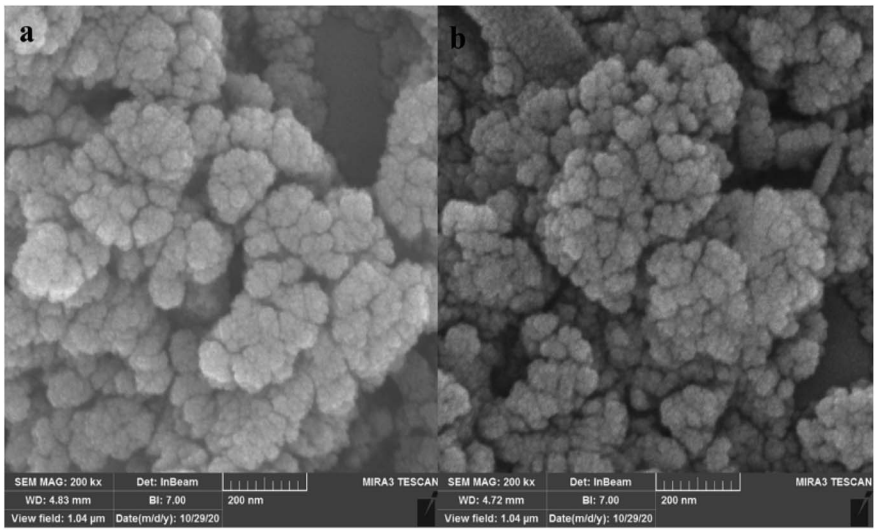

Fig. 4 FE-SEM images of Fe_3O_4/pectin/(Co/Cu)MOF.

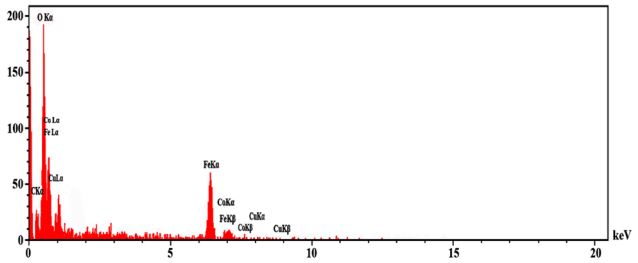

Fig. 5 EDS spectrum of Fe_3O_4/pectin/(Co/Cu)MOF.

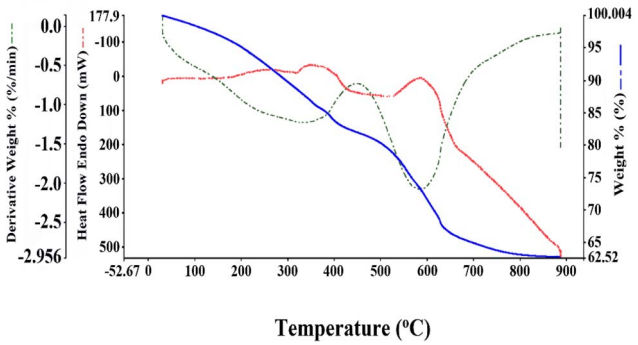

Fig. 6 STA thermogram of Fe_3O_4/pectin/(Co/Cu)MOF.

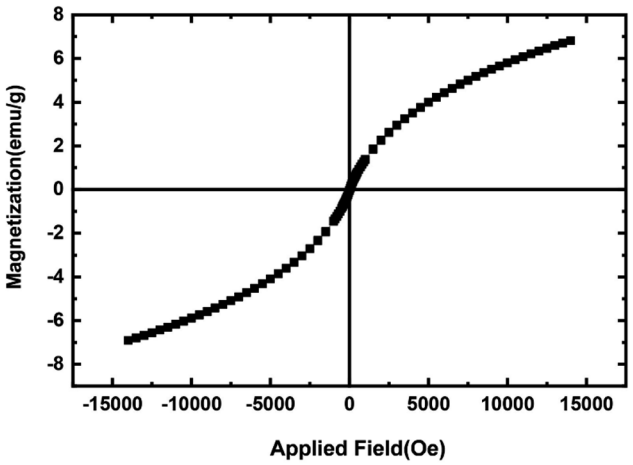

Fig. 7 VSM analysis of Fe_3O_4/pectin/(Co/Cu)MOF.

by temperature, and the best result was obtained at 85 °C (Table 1, entries 7–13). Additionally, various solvents such as THF, DMF, H_2O, ethanol, methanol, toluene (Table 1, entries 14–19), and solvent-free conditions were applied. The reaction yield under solvent-free conditions was higher in comparison with solvent conditions, and the reaction time was also shortened. Based on these studies, 25 mg of Fe_3O_4/pectin/(Co–Cu)MOF catalyst, 85 °C, and no solvent were chosen as optimum conditions. To further assess Fe_3O_4/pectin/(Co–Cu)MOF, its components separately [Fe_3O_4/pectin, Co-MOF, Cu-MOF and (Co–Cu)MOF] were used in the model reaction under the same conditions as the Fe_3O_4/pectin/(Co–Cu)MOF catalyst (Table 2). The results showed that the product with a lower yield was obtained using each of these components as a catalyst. Under these conditions, the activity of the Fe_3O_4/pectin/(Co–Cu)MOF was then investigated in the Biginelli reaction of several aldehyde substrates with ethyl acetoacetate and urea (Table 3). As seen, both electron-withdrawing and electron-releasing substituents on the aldehyde aryl ring were tolerated and reacted with ethyl acetoacetate and urea under optimized conditions. Strikingly, in all cases the corresponding products were isolated in high yields in pure crystal form. The results prove that the type and position of the substituent have no important effect on the activity of the catalyst. These observations confirm the high efficiency of the catalyst for the conversion of an extensive range of aldehyde substrates.

According to the recycling study, no significant reduction in the reactivity of the catalyst was observed. However, to verify the

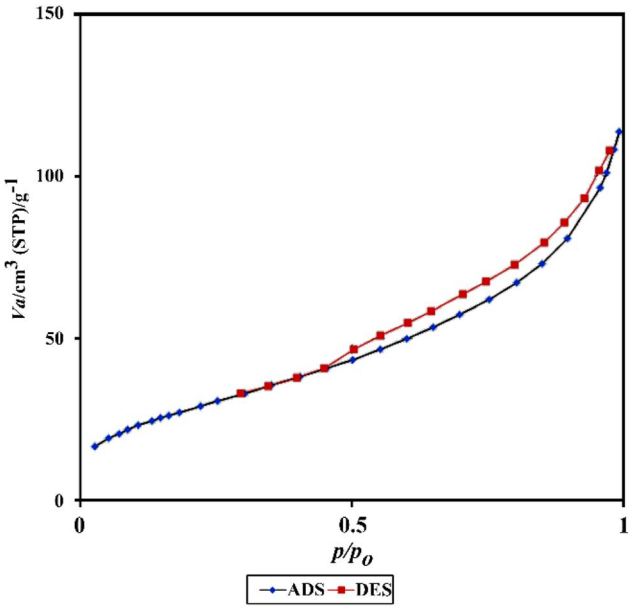

Fig. 8 N_2 adsorption–desorption isotherms of Fe_3O_4/pectin/(Co/Cu) MOF.

Table 1 Effect of catalyst loading, temperature and solvent in the synthesis of 3,4-dihydropyrimidinone[a]

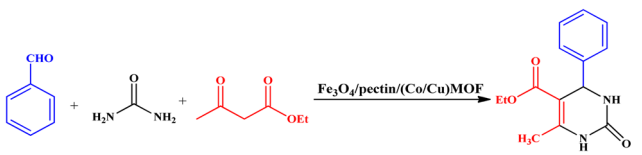

Entry	Catalyst (mg)	Solvent	T (°C)	Time (min)	Yield (%)
1	—	—	85	60	Trace
2	10	—	85	45	72
3	15	—	85	55	76
4	20	—	85	40	84
5	25	—	85	30	96
6	30	—	85	35	95
7	25	—	35	60	21
8	25	—	45	45	41
9	25	—	55	45	53
10	25	—	65	50	67
11	25	—	75	30	89
12	25	—	85	30	96
13	25	—	95	35	91
14	25	THF	85	50	73
15	25	DMF	85	65	62
16	25	H_2O	85	55	65
17	25	Ethanol	85	35	89
18	25	Methanol	85	35	66
19	25	Toluene	85	60	68
20	25	Solvent-free	85	30	96

[a] Reaction conditions: benzaldehyde (1 mmol), ethyl acetoacetate (1 mmol), urea (1.5 mmol), catalyst (25 mg).

extent of copper species leaching from the material during the reaction process, in the next investigation a hot filtration test was carried out for the reaction of benzaldehyde, urea, and ethyl

Table 2 Preparation of DHPM using Fe_3O_4/pectin, Co-MOF, Cu-MOF and (Co–Cu)MOF[a]

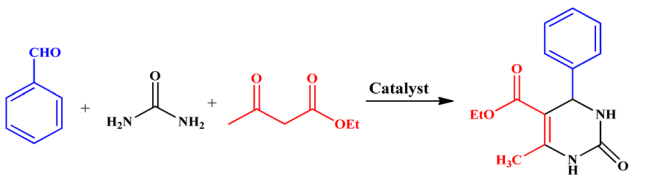

Entry	Catalyst	Time (min)	Yield (%)
1	Fe_3O_4/pectin	60	62
2	Co-MOF	60	73
3	Cu-MOF	60	61
4	(Co–Cu)MOF	60	82

[a] Reaction conditions: aldehyde (1 mmol), ethyl acetoacetate (1 mmol), urea (1.5 mmol), catalyst (25 mg). T = 85 °C.

acetoacetate after ~40% of the coupling reaction was completed. The filtrate was then transferred to another flask, and the reaction was continued under the same conditions as before. After 2 h, an additional conversion of only 5% was observed in the coupling reaction. Furthermore, atomic adsorption spectroscopy, performed for the filtrate, demonstrated that the amount of leached cobalt and copper is less than 1 ppm. This observation illustrates that the catalyst may operate in a heterogeneous manner.

To prove the heterogeneity of the catalyst, the filtration experiment of Fe_3O_4/pectin/(Co–Cu)MOF was performed. The catalyst was separated from the reaction mixture after 15 min,

Table 3 The Biginelli reaction of several aromatic aldehydes, ethyl acetoacetate and urea in the presence of Fe_3O_4/pectin/(Co/Cu)MOF catalyst[a]

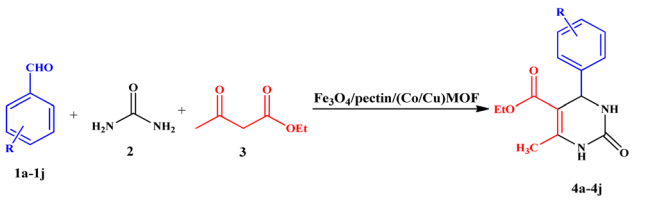

Entry	R	Time (min)	Yield (%)	m.p. (°C)
1 (**4a**)	H	30	96	202–204
2 (**4b**)	4-NO_2	20	98	202–203
3 (**4c**)	4-Cl	30	94	218–219
4 (**4d**)	2-Cl	35	92	221–223
5 (**4e**)	4-OMe	20	93	205–207
6 (**4f**)	2-OMe	20	91	266–268
7 (**4g**)	4-Me	45	92	217–219
8 (**4h**)	4-Br	35	93	212–214
9 (**4i**)	2-OH	25	85	218–220
10 (**4j**)	4-$CH(CH_3)_2$	45	76	210–212

[a] Reaction conditions: aldehyde (1 mmol), ethyl acetoacetate (1 mmol), urea (1.5 mmol), catalyst (25 mg). T = 85 °C.

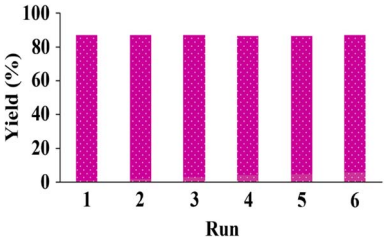

Fig. 9 Reusability of Fe_3O_4/pectin/(Co/Cu)MOF.

and the resulting filtrate was further stirred for 15 min. The conversion yield of the benzaldehyde remains unchanged for the filtrate, even at an extended time, indicating that the catalytic process is heterogeneous, and there is not any progress for the reaction in the homogeneous phase.

3.4. Reusability of Fe_3O_4/pectin/(Co–Cu)MOF

In the next study, the recycling performance of the Fe_3O_4/pectin/(Co–Cu)MOF nanocatalyst was tested in the condensation of benzaldehyde, ethyl acetoacetate, and urea under normal conditions. To this end, after the completion of the reaction, the mixture was filtered and thoroughly washed with hot ethanol. The recovered catalyst was then reused in the next run under the same conditions as the first run. More experiments were performed than before, and the results illustrated that the catalyst could be recovered and reused at least 5 times without significant lowering activity (Fig. 9). This observation strongly confirms the high recycling efficiency of the catalyst, which is a noteworthy property from economic and environmental points of view. The FT-IR, and SEM analyses of recycled Fe_3O_4/pectin/(Co/Cu)MOF (after the sixth run) were performed and the results were compared with the FT-IR, and SEM image of the fresh catalyst. The absorptions in the spectrum of recycled Fe_3O_4/pectin/(Co/Cu)MOF exhibited that the structure of the recovered catalyst was retained during the recycling process. Moreover, the amorphous nature and morphology of the recovered catalyst are similar to fresh catalyst demonstrating high stability of Fe_3O_4/pectin/(Co/Cu)MOF during the catalytic process (Fig. 10).

3.5. Comparison of the proposed catalyst with the previously reported catalysts for the Biginelli reaction

The comparison between the performance of the Biginelli reaction based on the Fe_3O_4/pectin/(Co–Cu)MOF catalyst and some previously reported catalysts involving the Biginelli reaction is listed in Table 4. It is found that Fe_3O_4/pectin/(Co–Cu)MOF exhibits advantages in terms of cost-effectiveness, simplicity, and short reaction time. Additionally, it has a short

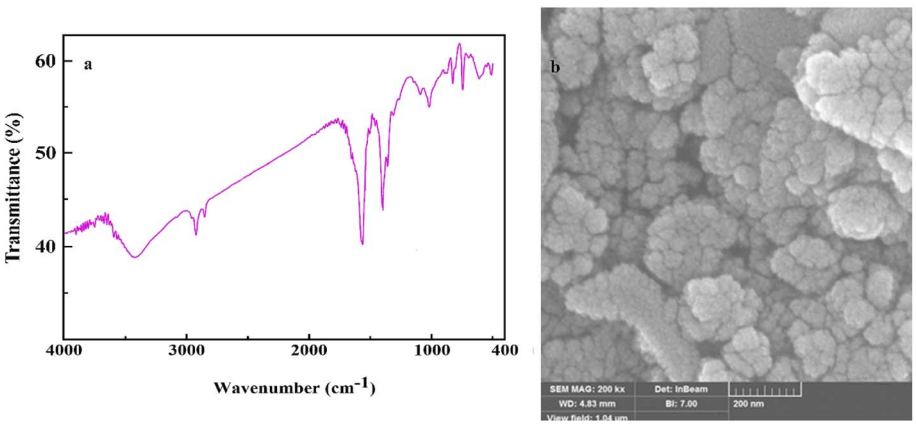

Fig. 10 FT-IR spectrum (a), and SEM image (b) of recycled Fe_3O_4/pectin/(Co–Cu)MOF.

Table 4 Comparison of the proposed catalyst with reported catalysts for the Biginelli reaction

Catalyst	Amount	Time	Solvent	T (°C)	Yield (%)	Ref.
Anionic Zn(II)-MOF	10 wt%	2 h	—	60	93	41
0.2$NbCl_5$-BMImCl	5 mol%	30 min	—	100	90	42
PTA@MIL-101	0.006 mmol	1 h	—	100	90	43
Cu-based MOF	0.1 mmol	2 h	—	60	86	44
Ompg-C_3N_4/SO_3H	30 mg	30 min	EtOH	Reflux	94	45
Ni-DDIA	0.005 mmol	30 min	—	80	84.6	7
BIL-SO_3H	2.5 mol%	3 h	EtOH	80	98	46
COF-IM-SO_3H	8.64 mg (1.0 mol%)	2.5 h	—	90	98	47
Fe_3O_4/pectin/(Co/Cu)MOF	25 mg	30 min	—	85	96	This work

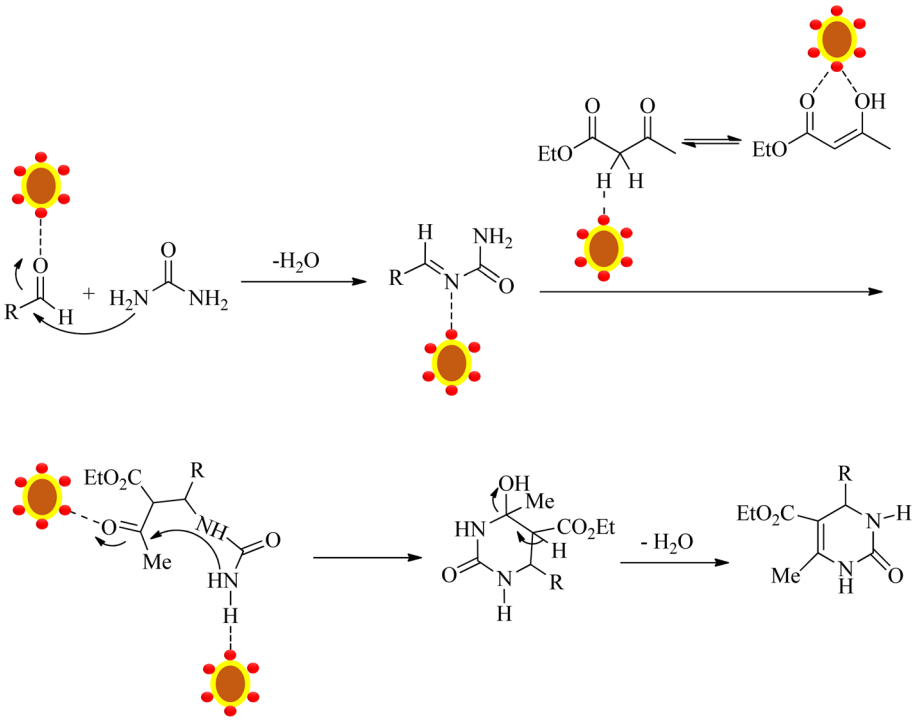

Scheme 1 Proposed mechanism for the construction of DHPMs catalyzed by Fe_3O_4/pectin/(Co–Cu)MOF.

reaction time and mild conditions in the Biginelli reaction compared with the literature.

In the proposed catalytic mechanism, *N*-acylimine intermediate was formed from the reaction of aldehyde and urea, which aldehyde activated by Lewis acidic [Co(II) and Cu(II)] and Brønsted acidic sites (the uncoordinated –COOH groups on the pectin surface). Consequently, the reaction of *N*-acylimine coordinated with Lewis acidic sites was carried out with enol of ethyl acetoacetate to provide ureide. The cyclization of ureide in the presence of catalyst gave the heterocyclic intermediate, which on dehydration affords the corresponding 3,4-dihydropyrimidin-2(1H)-one (DHPM) products (Scheme 1). Here Fe_3O_4/pectin/(Co–Cu)MOF has a large number of dispersed Brønsted acidic –COOH groups and Lewis acidic Co(II) and Cu(II) centers, which gives excellent catalytic performance to the reaction.

4. Conclusion

Bimetallic Co/Cu-MOF grown on Fe_3O_4/pectin was prepared and applied as a recoverable nanocatalyst for the one-pot synthesis of DHPM derivatives by the three-component condensation of diverse aldehydes, ethyl acetoacetate, and urea under solvent-free conditions. The catalyst was easily recovered and reused without a significant decrease in activity. The advantages of this catalyst system include short reaction time, low loading of catalyst, solvent-free conditions, and easy catalyst separation.

Data availability

All data generated or analyzed during this study are included in this published article.

Conflicts of interest

There are no conflicts to declare.

Acknowledgements

We are grateful to Yasouj University for financial assistance.

References

1 Y. Li, T. Tan, Y. Zhao, Y. Wei, D. Wang, R. Chen and L. Tao, Anticancer Polymers via the Biginelli Reaction, *ACS Macro Lett.*, 2020, **9**(9), 1249–1254.
2 A. de Fatima, T. C. Braga, L. da S. Neto, B. S. Terra, B. G. F. Oliveira, D. L. da Silva and L. V. Modolo, A Mini-Review on Biginelli Adducts with Notable Pharmacological Properties, *J. Adv. Res.*, 2015, **6**(3), 363–373.
3 R. Kaur, S. Chaudhary, K. Kumar, M. K. Gupta and R. K. Rawal, Recent Synthetic and Medicinal Perspectives of Dihydropyrimidinones: A Review, *Eur. J. Med. Chem.*, 2017, **132**, 108–134.
4 N. Yao, M. Lu, X. B. Liu, J. Tan and Y. L. Hu, Copper-Doped Mesoporous Silica Supported Dual Acidic Ionic Liquid as an Efficient and Cooperative Reusability Catalyst for Biginelli Reaction, *J. Mol. Liq.*, 2018, **262**, 328–335.
5 S. B. Moussa, J. Lachheb, M. Gruselle, B. Maaten, K. Kriis, T. Kanger, K. Tonsuaadu and B. Badraoui, Calcium, Barium and Strontium Apatites: A New Generation of Catalysts in the Biginelli Reaction, *Tetrahedron*, 2017, **73**(46), 6542–6548.

6 R. V. Patil, J. U. Chavan, D. S. Dalal, V. S. Shinde and A. G. Beldar, Biginelli Reaction: Polymer Supported Catalytic Approaches, *ACS Comb. Sci.*, 2019, **21**(3), 105–148.
7 S. Y. Zhao, Z. Y. Chen, N. Wei, L. Liu and Z. B. Han, Highly Efficient Cooperative Catalysis of Single-Site Lewis Acid and Brønsted Acid in A Metal–Organic Framework for the Biginelli Reaction, *Inorg. Chem.*, 2019, **58**(12), 7657–7661.
8 H. G. O. Alvim, D. L. J. Pinheiro, V. H. Carvalho-Silva, M. Fioramonte, F. C. Gozzo, W. A. da Silva, G. W. Amarante and B. A. D. Neto, Combined Role of the Asymmetric Counteranion-Directed Catalysis (ACDC) and Ionic Liquid Effect for the Enantioselective Biginelli Multicomponent Reaction, *J. Org. Chem.*, 2018, **83**(19), 12143–12153.
9 L. V. Chopda and P. N. Dave, Recent Advances in Homogeneous and Heterogeneous Catalyst in Biginelli Reaction from 2015–19: A Concise Review, *ChemistrySelect*, 2020, **5**(19), 5552–5572.
10 U. Patel, B. Parmar, P. Patel, A. Dadhania and E. Suresh, The Synthesis and Characterization of Zn(II)/Cd(II) Based MOFs by a Mixed Ligand Strategy: A Zn(II) MOF as a Dual Functional Material for Reversible Dye Adsorption and as a Heterogeneous Catalyst for the Biginelli Reaction, *Mater. Chem. Front.*, 2021, **5**, 304–314.
11 M. Barbero, S. Cadamuro and S. Dughera, A Brønsted Acid Catalysed Enantioselective Biginelli Reaction, *Green Chem.*, 2017, **19**, 1529–1535.
12 M. Neamtu, C. Nadejde, V. D. Hodoroaba, R. J. Schneider, L. Verestiuc and U. Panne, Functionalized Magnetic Nanoparticles: Synthesis, Characterization, Catalytic Application and Assessment of Toxicity, *Sci. Rep.*, 2018, **8**, 6278.
13 L. Mohammed, H. G. Gomaa, D. Ragab and J. Zhu, Magnetic Nanoparticles for Environmental and Biomedical Applications: A Review, *Particuology*, 2017, **30**, 1–14.
14 S. Singamaneni, V. N. Bliznyuk, C. Binek and E. Y. Tsymba, Magnetic Nanoparticles: Recent Advances in Synthesis, Self-Assembly and Applications, *J. Mater. Chem.*, 2011, **21**, 16819–16845.
15 S. Liu, B. Yu, S. Wang, Y. Shen and H. Cong, Preparation, Surface Functionalization and Application of Fe_3O_4 Magnetic Nanoparticles, *Adv. Colloid Interface Sci.*, 2020, **281**, 102165.
16 A. Bukowska, W. Bukowski, K. Hus, J. Depciuch and M. Parlinska-Wojtan, Synthesis and Characterization of New Functionalized Polymer-Fe_3O_4 Nanocomposite Particles, *Express Polym. Lett.*, 2017, **11**(1), 2–13.
17 E. Zare and Z. Rafiee, Magnetic Chitosan Supported Covalent Organic Framework/Copper Nanocomposite as an Efficient and Recoverable Catalyst for the Unsymmetrical Hantzsch Reaction, *J. Taiwan Inst. Chem. Eng.*, 2020, **116**, 205–214.
18 E. Zare and Z. Rafiee, Cellulose Stabilized Fe_3O_4 and Carboxylate-Imidazole and Co-Based MOF Growth as an Exceptional Catalyst for the Knoevenagel Reaction, *Appl. Organomet. Chem.*, 2020, **34**(4), 5516.
19 M. Azeem, F. Batool, N. Iqbal and I. ul-Haq, Chapter 1 – Algal-Based Biopolymers, *Algae Based Polymers, Blends, and Composites, Chemistry, Biotechnology and Materials Science*, Elsevier, 2017, 1–31.
20 C. Lara-Espinoza, E. Carvajal-Millan, R. Balandran-Quintana, Y. Lopez-Franco and A. Rascon-Chu, Pectin and Pectin-Based Composite Materials: Beyond Food Texture, *Molecules*, 2018, **23**(4), 942.
21 H. C. Zhou, J. R. Long and O. M. Yaghi, Introduction to Metal–Organic Frameworks, *Chem. Rev.*, 2012, **112**(2), 673–674.
22 M. Safaei, M. M. Foroughi, N. Ebrahimpoor, S. Jahani, A. Omidi and M. Khatami, A Review on Metal–Organic Frameworks: Synthesis and Applications, *TrAC, Trends Anal. Chem.*, 2019, **118**, 401–425.
23 T. A. Goetjen, J. Liu, Y. Wu, J. Sui, X. Zhang, J. T. Hupp and O. K. Farha, Metal–Organic Framework (MOF) Materials as Polymerization Catalysts: A Review and Recent Advances, *Chem. Commun.*, 2020, **56**, 10409–10418.
24 Q. Wang and D. Astruc, State of the Art and Prospects in Metal–Organic Framework (MOF)-based and MOF-Derived Nanocatalysis, *Chem. Rev.*, 2020, **120**(2), 1438–1511.
25 Q. Wang, Q. Gao, A. M. Al-Enizi, A. Nafady and S. Ma, Recent Advances in MOF-Based Photocatalysis: Environmental Remediation under Visible Light, *Inorg. Chem. Front.*, 2020, **7**, 300–339.
26 J. Yang and Y. W. Yang, Metal–Organic Frameworks for Biomedical Applications, *Small*, 2020, **16**(10), 1906846.
27 H. Li, L. Li, R.-B. Lin, W. Zhou, Z. Zhang, S. Xiang and B. Chen, Porous Metal–Organic Frameworks for Gas Storage and Separation: Status and Challenges, *EnergyChem*, 2019, **1**(1), 100006.
28 J. Ren, Y. Huang, H. Zhu, B. Zhang, H. Zhu, S. Shen, G. Tan, F. Wu, H. He, S. Lan, X. Xia and Q. Liu, Recent Progress on MOF-Derived Carbon Materials for Energy Storage, *Carbon Energy*, 2020, **2**(2), 176–202.
29 Q. Qian, P. A. Asinger, M. J. Lee, G. Han, K. M. Rodriguez, S. Lin, F. M. Benedetti, A. X. Wu, W. S. Chi and Z. P. Smith, MOF-Based Membranes for Gas Separations, *Chem. Rev.*, 2020, **120**(16), 8161–8266.
30 C. H. Chuang and C. W. Kung, Metal–Organic Frameworks toward Electrochemical Sensors: Challenges and Opportunities, *Electroanal*, 2020, **32**(9), 1885–1895.
31 G. E. Gomez, R. Marin, A. N. Carneiro Neto, A. M. P. Botas, J. Ovens, A. A. Kitos, M. C. Bernini, L. D. Carlos, G. J. A. A. Soler-Illia and M. Murugesu, Tunable Energy-Transfer Process in Heterometallic MOF Materials based on 2,6-Naphthalenedicarboxylate: Solid-State Lighting and Near-Infrared Luminescence Thermometry, *Chem. Mater.*, 2020, **32**(17), 7458–7468.
32 L. Chen, X. Zhang, X. Cheng, Z. Xie, Q. Kuang and L. Zheng, The Function of Metal–Organic Frameworks in the Application of MOF-Based Composites, *Nanoscale Adv.*, 2020, **2**, 2628–2647.
33 C. Liu, L. Lin, Q. Sun, J. Wang, R. Huang, W. Chen, S. Li, J. Wan, J. Zou and C. Yu, Site-Specific Growth of MOF-on-MOF Heterostructures with Controllable Nano-Architectures: Beyond the Combination of MOF Analogues, *Chem. Sci.*, 2020, **11**, 3680–3686.

34 J. Yu, C. Mu, B. Yan, X. Qin, C. Shen, H. Xue and H. Pang, Nanoparticle/MOF Composites: Preparations and Applications, *Mater. Horiz.*, 2017, **4**, 557–569.

35 Q. Yang, Q. Xu and H. L. Jiang, Metal–Organic Frameworks Meet Metal Nanoparticles: Synergistic Effect for Enhanced Catalysis, *Chem. Soc. Rev.*, 2017, **46**, 4774–4808.

36 L. Chen, H. F. Wang, C. Li and Q. Xu, Bimetallic Metal–Organic Frameworks and Their Derivatives, *Chem. Sci.*, 2020, **11**(21), 5369–5403.

37 X. He, D. R. Chen and W. N. Wang, Bimetallic Metal–Organic Frameworks (MOFs) Synthesized using the Spray Method for Tunable CO_2 Adsorption, *Chem. Eng. J.*, 2020, **382**, 122825.

38 X. Zhang, J. Luo, K. Wan, D. Plessers, B. Sels, J. Song, L. Chen, T. Zhang, P. Tang, M. J. Ramon, J. Arbiol and J. Fransaer, From Rational Design of a New Bimetallic MOF Family with Tunable Linkers to OER Catalysts, *J. Mater. Chem. A*, 2019, **7**(4), 1616–1628.

39 Y. Hu, J. Zhang, H. Huo, Z. Wang, X. Xu, Y. Yang, K. Lin and R. Fan, One-Pot Synthesis of Bimetallic Metal–Organic Frameworks (MOFs) as Acid–Base Bifunctional Catalysts for Tandem Reaction, *Catal. Sci. Technol.*, 2020, **10**(2), 315–322.

40 S. H. Guo, X. J. Qi, H. M. Zhou, J. Zhou, X. H. Wang, M. Dong, X. Zhao, C. Y. Sun, X. L. Wang and Z. M. Su, A Bimetallic-MOF Catalyst for Efficient CO_2 Photoreduction from Simulated Flue Gas to Value-Added Formate, *J. Mater. Chem. A*, 2020, **8**(23), 11712–11718.

41 A. Verma, D. De, K. Tomar and P. K. Bharadwaj, An Amine Functionalized Metal–Organic Framework as an Effective Catalyst for Conversion of CO_2 and Biginelli Reactions, *Inorg. Chem.*, 2017, **56**(16), 9765–9771.

42 M. C. Santos, M. Uemi, N. S. Goncalves, M. A. Bizeto and F. F. Camilo, Niobium Chloride in 1-*n*-Butyl-3-methylimidazolium Chloride Ionic Liquid as a Catalyst for Biginelli Reaction, *J. Mol. Struct.*, 2020, **1220**, 128653.

43 M. Saikia, D. Bhuyana and L. Saikiaa, Keggin Type Phosphotungstic Acid Encapsulated Chromium (III) Terephthalate Metal Organic Framework as Active Catalyst for Biginelli Condensation, *Appl. Catal., A*, 2015, **505**, 501–506.

44 T. K. Pal, D. De, S. Senthilkumar, S. Neogi and P. K. Bharadwaj, A Partially Fluorinated, Water-Stable Cu(II)-MOF Derived via Transmetalation: Significant Gas Adsorption with High CO_2 Selectivity and Catalysis of Biginelli Reactions, *Inorg. Chem.*, 2016, **55**(16), 7835–7842.

45 M. A. Douzandegi Fard, H. Ghafuri and A. Rashidizadeh, Sulfonated Highly Ordered Mesoporous Graphitic Carbon Nitride as a Super Active Heterogeneous Solid Acid Catalyst for Biginelli Reaction, *Microporous Mesoporous Mater.*, 2019, **274**, 83–93.

46 G. P. Zhang, D. Y. Tian and W. M. Shi, Efficient Catalytic Synthesis of 3,4-Dihydropyrimidin-2-ones/Thiones via Little Acidic Ionic Liquid Combined with Rapid Heating Ways, *J. Heterocycl. Chem.*, 2018, **55**(11), 2522–2531.

47 B. J. Yao, W. X. Wu, L. G. Ding and Y. B. Dong, Sulfonic Acid and Ionic Liquid Functionalized Covalent Organic Framework for Efficient Catalysis of the Biginelli Reaction, *J. Org. Chem.*, 2021, **86**(3), 3024–3032.